

Elastic registration of brain cine-MRI sequences using MLSDO dynamic optimization algorithm

Julien Lepagnet, Amir Nakib, Hamouche Oulhadj and Patrick Siarry

Abstract In this chapter, we propose to use a dynamic optimization algorithm to assess the deformations of the wall of the third cerebral ventricle in the case of a brain cine-MR imaging. In this method, an elastic registration process is applied to a 2D+t cine-MRI sequence of a region of interest (*i.e.* lamina terminalis). This registration process consists of optimizing an objective function that can be considered as dynamic. Thus, a dynamic optimization algorithm, called MLSDO, is used to accomplish this task. The obtained results are compared to those of several well-known static optimization algorithms. This comparison shows the efficiency of MLSDO, and the relevance of using a dynamic optimization algorithm to solve this kind of problems.

1 Introduction

Hydrocephalus is a medical condition in which there is an abnormal accumulation of cerebrospinal fluid in the ventricles, or cavities, of the brain. This may cause increased intracranial pressure inside the skull and progressive enlargement of the head, convulsion, tunnel vision, and mental disability. Hydrocephalus can also cause death. Hydrocephalus may be suggested by symptoms; however, imaging studies of the brain are the mainstay of diagnosis. In this paper, we focus on a method based on cine-MRI sequences to facilitate this diagnosis, and to assist neurosurgeons in the treatment of hydrocephalus. This method makes use of the dynamic optimization paradigm.

Université Paris-Est Créteil (UPEC)
LISSI, E.A. 3956
61 avenue du Général de Gaulle, 94010 Créteil, France
e-mail: siarry@u-pec.fr

Recently, optimization in dynamic environments has attracted a growing interest, due to its practical relevance. Almost all real-world problems are time dependent or dynamic, *i.e.* their objective function changes over the time. For dynamic environments, the goal is not only to locate the global optimum, but also to track it as closely as possible over the time. Then, a dynamic optimization problem can be expressed as in (1), where $f(\mathbf{x}, t)$ is the objective function of a minimization problem, $h_j(\mathbf{x}, t)$ denotes the j^{th} equality constraint and $g_k(\mathbf{x}, t)$ denotes the k^{th} inequality constraint. All of these functions may change over time (iterations), as indicated by the dependence on the time variable t .

$$\begin{aligned} \min & f(\mathbf{x}, t) \\ \text{s.t.} & h_j(\mathbf{x}, t) = 0 \text{ for } j = 1, 2, \dots, u \\ & g_k(\mathbf{x}, t) \leq 0 \text{ for } k = 1, 2, \dots, v \end{aligned} \quad (1)$$

In this chapter, we focus on a dynamic optimization problem with time constant constraints. We propose to apply the *Multiple Local Search algorithm for Dynamic Optimization* (MLSDO) [14] to the registration of sequences of images.

Image registration is the process of overlaying two or more images of the same scene taken at different times, from different viewpoints, and/or by different sensors. It is a critical step in all image analysis tasks in which the final information is gained from the combination of various data sources like in image fusion or change detection.

It geometrically aligns two images: the source and the target images. It is done by determining a transformation that maps the target image to the source one. Thus, registering a sequence of images consists of determining, for each couple of successive images, the transformation that makes the first image of the couple match the following image.

Comprehensive surveys of the registration approaches are available in the literature, we can cite [8, 24, 36]. Registration approaches can be roughly based on:

- geometric image features (geometric registration), such as points, edges and surfaces ;
- measures computed from the image grey values (intensity based registration), such as mutual information.

In the domain of medical imaging, a satisfactory solution can be found in many cases by using a rigid or an affine transformation (deformation model applied to the target image), *i.e.* the target image is only translated, rotated and scaled to match the source image [28]. Elastic registration is required to register inter-patient images or regions containing non-rigid objects. The goal is to remove structural variation between the two images to be registered. As stated in [24], most applications represent elastic transformations in terms of a local vector displacement (disparity) field, or as polynomial transformations in terms of the old coordinates.

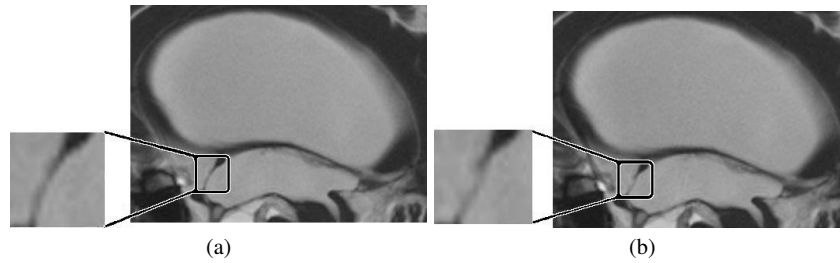


Fig. 1 Two images from a brain cine-MRI sequence: (a) first image of the sequence, (b) sixth image of the sequence.

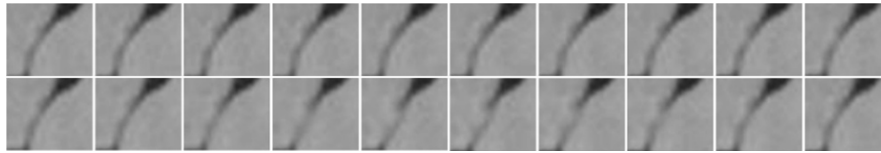


Fig. 2 A sequence of cine-MR images of the region of interest.

In the problem at hand, each image of the region of interest (*i.e.* lamina terminalis) is extracted from a brain cine-MRI sequence of 20 images. This sequence corresponds to 80% of a R-R cardiac cycle, more details about the acquisition procedure are given in [28]. An example of two images extracted from a brain cine-MRI sequence is presented in Figure 1. Hence, each sequence is composed of 20 MR images. An example of sequence is illustrated in Figure 2. The goal is to register each couple of successive images of the sequence. Hence, for a sequence of 20 images, 19 couples of successive images have to be registered. Then, the transformations that result from this matching operation can be used to assess the deformation movements of the third cerebral ventricle.

Several papers are proposed in the literature about the analysis and quantification of cardiac movements, we can cite those recently published [6, 7, 33]. In our case, the single approach that deals with the problem at hand is [28], because of the recent appearance of the acquisition method of the images. The main difference between the problem at hand and the cardiac problem lies in the amplitude of the movements of the ventricles. Indeed, the amplitude of the cardiac ventricle movements is higher than the amplitude of the cerebral ventricle movements. In this chapter, we propose a method inspired from [28] to assess the movements of a region of interest (ROI). Besides, another contribution of the present work is to show the importance of the use of dynamic optimization algorithms for brain cine-MRI registration.

The rest of this chapter is organized as follows. In section 2, the method proposed to register sequences of images is described. In section 3, the MLSDO algorithm and its use for the problem at hand are presented. In section 4, a comparison of

the results obtained by MLSDO on this problem to the ones of several well-known static optimization algorithms is performed. This comparison shows the relevance of using MLSDO on this problem. Finally, a conclusion and the works under progress are given in section 5.

2 The registration process

A method inspired from [28] is proposed in this chapter to evaluate the movement in sequences of cine-MR images. This operation is required in order to assess the movements in the ROI over time. In [28], a segmentation process is performed on each image of the sequence, to determine the contours (as a set of points) of the walls of the third cerebral ventricle. Then, a geometric registration of each successive contours is performed, based on an affine deformation model. In the present work, we propose to use an intensity based registration instead of a geometric registration process. This way, we do not have to use a segmentation process anymore. Moreover, to evaluate the pulsatile movements of the third cerebral ventricle more precisely, an elastic deformation model is used in this chapter.

Let Im_1 and Im_2 be two successive images of the sequence. Let the transpose of a matrix A be denoted by A^T . Then, we assume that a transformation T_Φ allows to match Im_1 with $Im'_1 = T_\Phi(Im_2)$ and, for every pixel $o_2 = (x_2 \ y_2)^T$ of Im_2 , it is defined by:

$$\begin{aligned} x'_1 &= c_1 x_2^2 + c_2 y_2^2 + c_3 x_2 y_2 + (c_4 |c_4| + 1) x_2 + c_5 |c_5| y_2 + (c_6)^3 \\ y'_1 &= c_7 x_2^2 + c_8 y_2^2 + c_9 x_2 y_2 + c_{10} |c_{10}| x_2 + (c_{11} |c_{11}| + 1) y_2 + (c_{12})^3 \end{aligned} \quad (2)$$

where $o'_1 = (x'_1 \ y'_1)^T = T_\Phi(o_2)$. The set of parameters $\Phi = \{c_1, c_2, \dots, c_{12}\}$ is estimated through the maximization of the following criterion:

$$C(\Phi) = \frac{NMI(\Phi)}{P(\Phi) + 1} \quad (3)$$

where $NMI(\Phi)$ computes the normalized mutual information [32] of Im_1 and Im'_1 ; $P(\Phi)$ is part of a regularization term that penalizes large deformations of Im_2 , as we are dealing with slight movements in the ROI. Besides, as the size of the ROI is not constant, we have to normalize the coordinates of the pixels. Then, we make the pixels in the ROI range in the interval $[-0.5, 0.5]$. The use of this interval transforms discrete coordinates of the pixels into continuous ones, as defined in (4). This interval was determined empirically, and it is well fitted to the regularization term, and to the transformation model used. Among a set of possible intervals, this one leads to the best results, in terms of accuracy and speed. $NMI(\Phi)$ and $P(\Phi)$ are defined in (5) and (6), respectively.

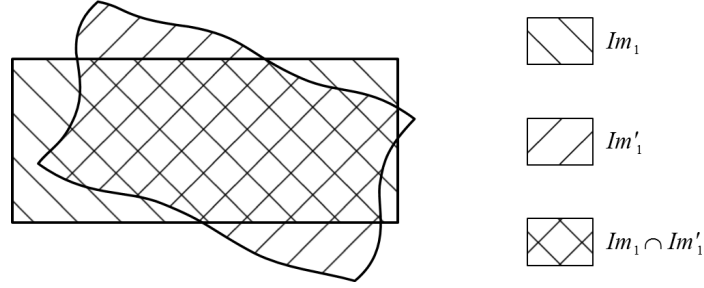


Fig. 3 Overlapping area ($Im_1 \cap Im'_1$) of the source image (Im_1) and the transformed target image (Im'_1) in the registration of a couple of successive images of a sequence.

$$\begin{aligned} x &= \frac{X}{S_X - 1} - 0.5 \\ y &= \frac{Y}{S_Y - 1} - 0.5 \end{aligned} \quad (4)$$

where $X \in \{1, 2, \dots, S_X - 1\}$ and $Y \in \{1, 2, \dots, S_Y - 1\}$ are the discrete coordinates of a pixel ; x and y are the normalized coordinates of this pixel in $[-0.5, 0.5]$.

$$NMI(\Phi) = \frac{H(Im_1) + H(Im'_1)}{H(Im_1, Im'_1)} \quad (5)$$

$$P(\Phi) = \max_{o_2 \in Im_1 \cap Im'_1} (o_2 - o'_1)^T (o_2 - o'_1) \quad (6)$$

where $Im_1 \cap Im'_1$ is the overlapping area of Im_1 and Im'_1 (see Figure 3) ; $H(Im_1)$ and $H(Im'_1)$ compute the Shannon entropy of Im_1 and Im'_1 , respectively, in their overlapping area ; $H(Im_1, Im'_1)$ computes the joint Shannon entropy of Im_1 and Im'_1 , in their overlapping area. They are defined as follows:

$$H(Im_1) = - \sum_{i=0}^{L-1} p(i) \log_2(p(i)) \quad (7)$$

$$H(Im'_1) = - \sum_{j=0}^{L-1} p'(j) \log_2(p'(j)) \quad (8)$$

$$H(Im_1, Im'_1) = - \sum_{i=0}^{L-1} \sum_{j=0}^{L-1} p(i, j) \log_2(p(i, j)) \quad (9)$$

where L is the number of possible grey values that a pixel can take ; $p(i)$, $p'(j)$ and $p(i, j)$ are the probability of the pixel intensity i in Im_1 , the probability of the pixel intensity j in Im'_1 and the joint probability of having a pixel intensity i in Im_1 and j in Im'_1 , respectively. They are defined as follows:

$$p(i) = \frac{g(i)}{\sum_{k=0}^{L-1} g(k)} \quad (10)$$

$$p'(j) = \frac{g'(j)}{\sum_{l=0}^{L-1} g'(l)} \quad (11)$$

$$p(i, j) = \frac{g(i, j)}{\sum_{k=0}^{L-1} \sum_{l=0}^{L-1} g(k, l)} \quad (12)$$

where $g(i)$ is the histogram of the overlapping area of Im_1 (occurrence of gray level i in Im_1); $g'(j)$ is the histogram of the overlapping area of Im'_1 (occurrence of gray level j in Im'_1); $g(i, j)$ is the joint histogram of the overlapping area of Im_1 and Im'_1 (occurrence of having a grey value equal to i in Im_1 and to j in Im'_1 , see equation (13)). However, in this work, we apply a low-pass filter to these histograms, using a convolution with a Gaussian function, in order to accelerate the convergence of the optimization process (the number of evaluations of the objective function performed during the optimization process is reduced by 10.4%). Applying this filter reduces indeed the number of local optima in the objective function, by smoothing it. An illustration of the histogram of an MR image from a sequence, and of its corresponding smoothed histogram, are illustrated in Figure 4.

In (13), the cardinal function is denoted by *card*, and the functions $Im_1(o)$ and $Im'_1(o)$ return the grey values of a given pixel o in Im_1 and Im'_1 , respectively.

$$g(i, j) = \text{card} \{o \in Im_1 \cap Im'_1, Im_1(o) = i \wedge Im'_1(o) = j\} \quad (13)$$

The registration problem can be formulated as an optimization problem defined by:

$$\max C(\Phi) \quad (14)$$

3 The MLSDO algorithm

In this section, MLSDO and its use on the problem at hand are described. At first, the algorithm is presented. Then, the dynamic objective function proposed for the problem at hand is described. Afterwards, the parameter fitting of MLSDO is given to solve this problem.

3.1 Description of the algorithm

MLSDO uses several local searches, each one performed in parallel with the others, to explore the search space, and to track the found optima over the changes in the

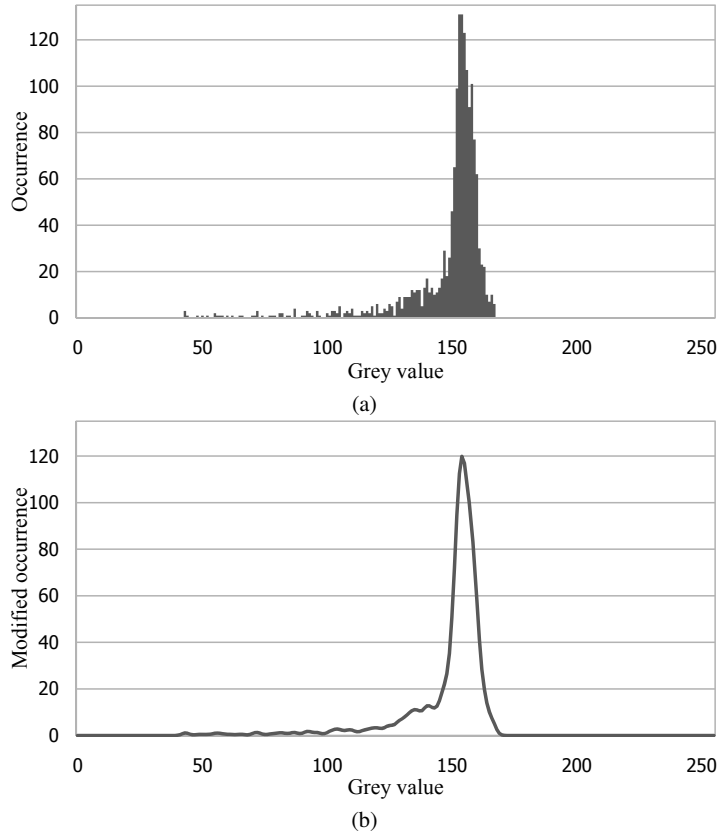


Fig. 4 Illustration of the histogram of an MR image: (a) original histogram, (b) smoothed histogram used to accelerate the optimization process.

objective function. These local searches consist of moving step-by-step in the search space, from a current solution to its best neighbor one, until a stopping criterion is satisfied, reaching thus a local optimum. Each local search is performed by an agent, and all the agents are coordinated by a dedicated module (the coordinator). Two types of agents exist in MLSDO: the exploring agents (to explore the search space in order to discover the local optima), and the tracking agents (to track the found local optima over the changes in the objective function). The local searches performed by the exploring agents have a greater initial step size than the one of the tracking agents, because the exploring agents have to widely explore the search space. The strategies used to coordinate these local search agents enable the fast convergence to well diversified optima, in order to quickly react to a change and find the global optimum. Especially, each agent performs its local search in an exclusive area of the search space : an exclusion radius is attributed to each agent. This way, if several agents converge to a same local optimum, then only one of them can continue to

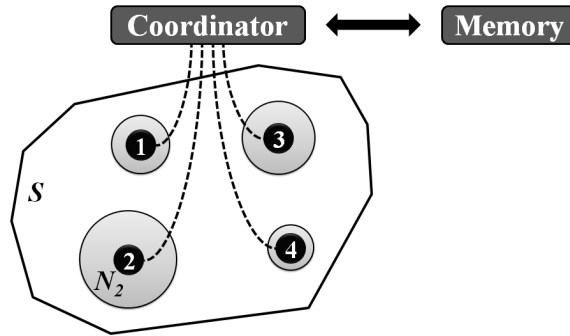


Fig. 5 Overall scheme of MLSDO.

converge to this local optimum : all the other conflicting agents are reinitialized elsewhere in the search space. Another important strategy is the use of two levels of precision in the stopping criterion of the local searches of the agents. In this way, we prevent the fine-tuning of low quality solutions, which could lead to a waste of fitness function evaluations; only the best solution found by MLSDO is fine-tuned. Furthermore, the local optima found during the optimization process are archived, to accelerate the detection of the global optimum after a change in the objective function. These archived optima are used as initial solutions of the local searches performed by the tracking agents. The overall scheme of MLSDO is illustrated in Figure 5, where the local search agents are depicted by the numbered black-filled circles in the search space S , and the neighborhood of the i^{th} agent is denoted by N_i . More details about this algorithm are in [14].

MLSDO has been compared to other dynamic optimization algorithms using two of the main benchmarks : the Moving Peaks Benchmark (MPB) [4] and the Generalized Dynamic Benchmark Generator (GDBG) [17, 19].

Among the three configurations of MPB proposed in [4], called scenarios, we chose the most used one (scenario 2). MPB scenario 2 is characterized by a five dimensional search space with ten local optima. A change occurs in the objective function of MPB every 5000 evaluations, and the total number of changes is equal to 100.

The configuration of GDBG used in this chapter was used during the CEC'2009 competition on dynamic optimization. GDBG is made of 49 test cases that correspond to the combinations of six problems with seven change scenarios. One of these change scenarios involves varying the dimension of the search space between 5 and 15 dimensions. The dimension used in the other change scenarios is fixed to 10. In GDBG, a change occurs in the objective function of a test case every $10000 \times d$ evaluations, where d is the dimension of the search space. The total number of changes for a test case is equal to 60.

The comparison, on MPB, of MLSDO with the other leading optimization algorithms in dynamic environments is summarized in Table 1. These competing al-

Algorithm	Offline error
Moser and Chiong, 2010 [26]	0.25 ± 0.08
MLSDO	0.35 ± 0.06
Novoa <i>et al.</i> , 2009 [29]	0.40 ± 0.04
Lepagnot <i>et al.</i> , 2009 [15, 16]	0.59 ± 0.10
Moser and Hendtlass, 2007 [26, 27]	0.66 ± 0.20
Yang and Li, 2010 [34]	1.06 ± 0.24
Liu <i>et al.</i> , 2010 [21]	1.31 ± 0.06
Lung and Dumitrescu, 2007 [22]	1.38 ± 0.02
Bird and Li, 2007 [1]	1.50 ± 0.08
Lung and Dumitrescu, 2008 [23]	1.53 ± 0.01
Blackwell and Branke, 2006 [3]	1.72 ± 0.06
Mendes and Mohais, 2005 [25]	1.75 ± 0.03
Li <i>et al.</i> , 2006 [20]	1.93 ± 0.06
Blackwell and Branke, 2004 [2]	2.16 ± 0.06
Parrott and Li, 2006 [30]	2.51 ± 0.09
Du and Li, 2008 [10]	4.02 ± 0.56

Table 1 Comparison of MLSDO with competing algorithms on MPB using standard settings (scenario 2).

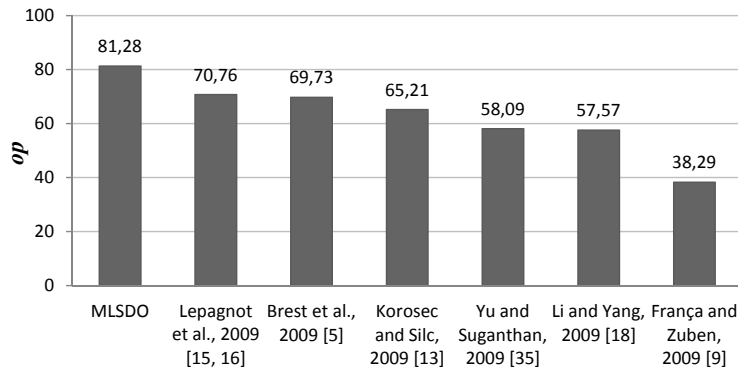


Fig. 6 Comparison of MLSDO with competing algorithms on GDBG.

gorithms are the only ones that we found suitable for comparison in the literature, *i.e.*, they are tested by their authors using the most commonly used configuration of MPB. The *offline errors* (a measure of performance used in MPB, see [4]) and the standard deviations are given, and the algorithms are sorted from the best to the worst. Results are averaged on 50 runs of the tested algorithms. As we can see, MLSDO is the second ranked algorithm in terms of offline error.

The comparison, on GDBG, of MLSDO with the other leading optimization algorithms in dynamic environments is summarized in Figure 6. The algorithms are ranked according to their *overall performance* (a score between 0 and 100, denoted by *op*, see [19]). As we can see, MLSDO is the first ranked algorithm on this benchmark.

3.2 Cine-MRI registration as a dynamic optimization problem

The registration of a cine-MRI sequence can be seen as a dynamic optimization problem. Then, the dynamic objective function optimized by MLSDO changes according to the following rules:

- The criterion in (3) has to be maximized for each couple of successive images, as we are in the case of a sequence, then the optimization criterion becomes:

$$C(\Phi(t)) = \frac{NMI(\Phi(t))}{P(\Phi(t)) + 1} \quad (15)$$

where t is the index of the current couple of images in the sequence. $\Phi(t)$, $NMI(\Phi(t))$ and $P(\Phi(t))$ are the same as Φ , $NMI(\Phi)$ and $P(\Phi)$ defined before, respectively, but here are dependent on the couple of images.

- Then, the dynamic optimization problem is defined by:

$$\max C(\Phi(t)) \quad (16)$$

- If the current best solution (transformation) found for the couple t cannot be improved anymore (according to a stagnation criterion), the next couple $(t + 1)$ is treated.
- The stagnation criterion of the registration of a couple of successive images is satisfied if no significant improvement (higher than 1E-5) in the current best solution is observed during 5000 successive evaluations of the objective function.
- Thus, the end of the registration of a couple of images and the beginning of the registration of the next one constitute a change in the objective function.

3.3 Parameter fitting of MLSDO

Table 2 summarizes the six parameters of MLSDO that the user has to define. These values will be used to perform the experiments reported in the following section.

In this table, the values given are suitable for the problem at hand, and they were fixed experimentally. Among several sets of values for the parameters, we selected the one that minimizes the number of evaluations performed. One can see that only one exploring agent is used to solve this problem. It is indeed sufficient for this problem, and using more than one exploring agent increases the number of evaluations required to register a sequence. However, using more than one exploring agent can improve the performance of MLSDO on other problems.

Name	Type	Interval	Value	Short description
r_l	real	$(0, r_e)$	0.005	initial step size of tracking agents
r_e	real	$(0, 1]$	0.1	exclusion radius of the agents, and initial step size of exploring agents
δ_{ph}	real	$[0, \delta_{pl}]$	1E-5	highest precision parameter of the stopping criterion of the agents local searches
δ_{pl}	real	$[\delta_{ph}, +\infty)$	1E-4	lowest precision parameter of the stopping criterion of the agents local searches
n_a	integer	$[1, 10]$	1	maximum number of exploring agents
n_c	integer	$[0, 20]$	2	maximum number of tracking agents created after the detection of a change

Table 2 MLSDO parameter setting for the problem at hand.

4 Experimental results and discussion

The registrations of two couples of slightly different images are illustrated in Figures 7 and 8, and the registrations of two couples of significantly different images are illustrated in Figures 9 and 10. As we can see in Figures 7(e) and 7(f), as well as in Figures 8(e) and 8(f), if the movements in the ROI are not significant, then only noise appears in the difference images. Hence, the transformation used to register the couple of images (Figures 7(d) and 8(d)) does not deform the second image of the couple significantly. On the other hand, significant movements in the ROI leave an important white trail in the difference images, as illustrated in Figures 9(e) and 10(e). Then, a significant transformation (Figure 9(d) and 10(d)) has to be applied in order to eliminate the white trail (see Figure 9(f) and 10(f)).

A comparison between the results obtained by MLSDO and those obtained by several well-known static optimization algorithms is presented in this section. These algorithms, and their parameter setting, empirically fitted to the problem at hand, are defined below (see references for more details on these algorithms and their parameter fitting):

- CMA-ES (*Covariance Matrix Adaptation Evolution Strategy*) [12] using the recommended parameter setting, except for the initial step size σ , set to $\sigma = 0.5$. The population size λ of children and the number of selected individuals μ are set to $\lambda = 11$ and $\mu = 5$;
- SPSO-07 (*Standard Particle Swarm Optimization* in its 2007 version) [11] using the recommended parameter setting, except for the number S of particles ($S = 12$) and for the parameter K used to generate the particles neighborhood ($K = 8$) ;
- DE (*Differential Evolution*) [31] using the “DE/target-to-best/1/bin” strategy, a number of parents equal to $NP = 30$, a weighting factor $F = 0.8$, and a crossover constant $CR = 0.9$.

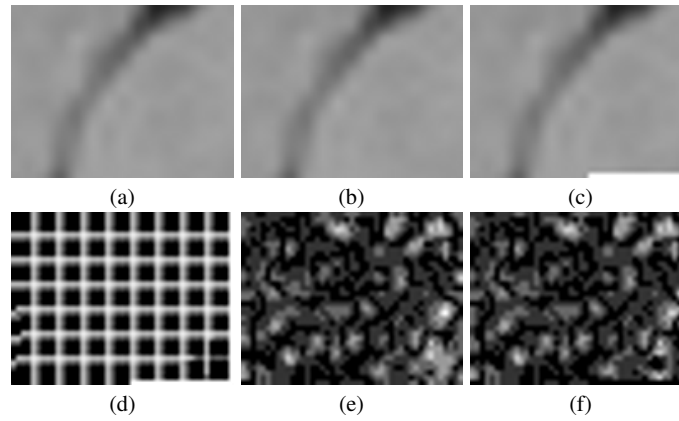


Fig. 7 Illustration of the registration of a couple of slightly different images of a sequence: (a) the first image of the couple, (b) the second image of the couple, (c) the second image after applying the found transformation to it, (d) illustration showing the transformation applied on the second image of the couple to register it, (e) illustration showing the difference, in the intensity of the pixels, between the two images of the couple: a black pixel indicates that the intensities of the corresponding pixels in the images are the same, and a white pixel indicates the highest difference between the images, (f) illustration showing the difference, in the intensity of the pixels, between the first image and the transformed second image.

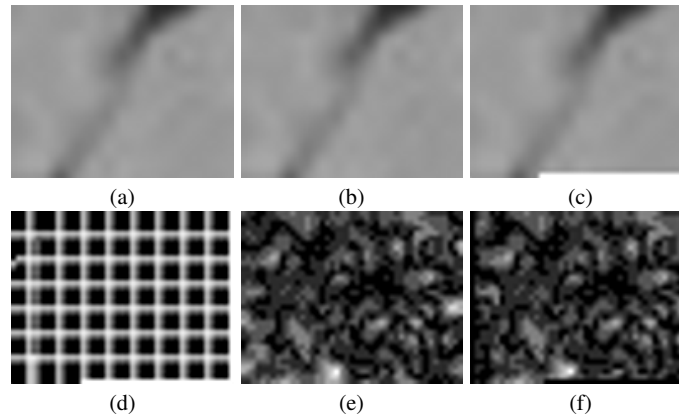


Fig. 8 Illustration of the registration of another couple of slightly different images of a sequence, in the same way as in Figure 7.

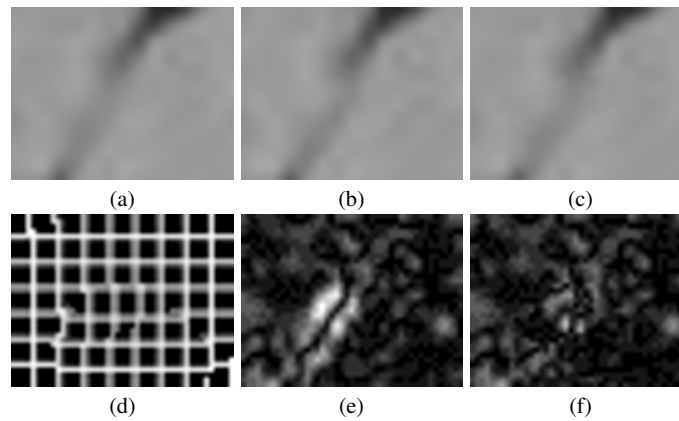


Fig. 9 Illustration of the registration of a couple of significantly different images of a sequence: (a) the first image of the couple, (b) the second image of the couple, (c) the second image after applying the found transformation to it, (d) illustration showing the transformation applied on the second image of the couple to register it, (e) illustration showing the difference, in the intensity of the pixels, between the two images of the couple: a black pixel indicates that the intensities of the corresponding pixels in the images are the same, and a white pixel indicates the highest difference between the images, (f) illustration showing the difference, in the intensity of the pixels, between the first image and the transformed second image.

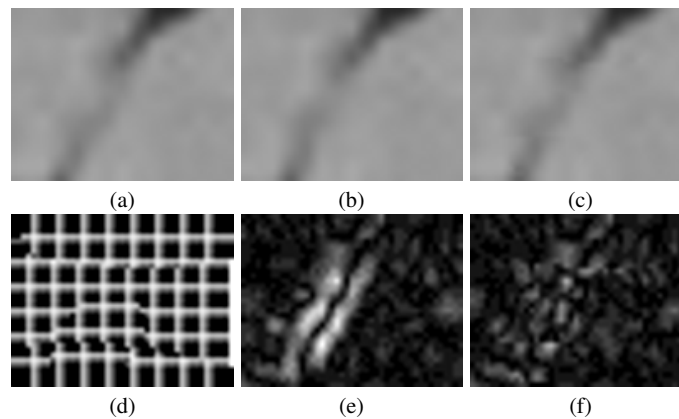


Fig. 10 Illustration of the registration of another couple of significantly different images of a sequence, in the same way as in Figure 9.

t	c_1	c_2	c_3	c_4	c_5	c_6	c_7	c_8	c_9	c_{10}	c_{11}	c_{12}	$C^*(\Phi(t))$
1	0.039	-0.022	0.005	0.105	-0.034	0.139	-0.039	0.017	0.025	0.091	0.132	0.090	1.199
2	-0.005	-0.029	0.025	0.085	-0.014	0.203	0.077	0.055	0.051	0.068	-0.077	-0.264	1.201
3	0.055	0.063	0.048	0.094	-0.104	-0.239	0.068	0.000	0.000	-0.074	-0.083	-0.256	1.192
4	0.021	0.031	-0.001	0.095	-0.077	-0.223	0.025	0.013	0.006	0.081	-0.144	-0.246	1.195
5	0.063	0.000	0.003	-0.074	-0.026	-0.089	-0.026	0.041	0.011	0.100	0.145	-0.128	1.218
6	0.002	-0.063	-0.033	-0.115	0.034	0.224	-0.019	-0.027	0.024	0.015	0.087	0.258	1.209
7	0.013	-0.092	0.016	0.036	0.080	0.253	-0.060	-0.045	-0.033	-0.077	0.131	0.247	1.208
8	0.003	-0.068	-0.004	-0.023	0.117	0.238	-0.069	-0.047	-0.032	-0.078	0.131	0.247	1.195
9	0.065	-0.020	-0.007	0.044	0.061	-0.046	-0.064	-0.047	-0.023	-0.081	0.131	0.251	1.201
10	0.050	-0.004	-0.017	0.072	0.056	-0.061	0.051	0.005	0.011	-0.052	0.135	-0.043	1.216
11	0.050	0.000	-0.012	-0.004	0.073	-0.053	-0.059	0.047	0.002	0.099	0.164	-0.178	1.216
12	0.060	0.011	0.003	0.080	-0.033	-0.191	-0.024	0.032	0.036	-0.068	0.108	0.048	1.225
13	0.042	0.000	0.000	0.050	-0.018	-0.060	-0.023	0.016	0.002	-0.085	-0.064	-0.218	1.232
14	0.064	-0.005	0.000	0.094	-0.021	-0.199	-0.016	0.075	0.065	-0.039	0.065	-0.210	1.232
15	0.025	-0.008	0.042	0.049	-0.072	0.172	0.037	0.029	0.000	0.104	0.107	-0.037	1.235
16	0.060	0.007	0.003	0.082	-0.026	-0.191	-0.024	0.032	0.034	-0.063	0.111	-0.049	1.216
17	0.050	-0.005	0.000	0.021	0.010	-0.071	-0.025	0.047	0.052	0.018	0.080	-0.170	1.226
18	0.052	-0.005	-0.017	0.083	0.108	-0.121	-0.018	0.042	-0.001	0.071	0.075	0.149	1.225
19	-0.006	0.056	-0.011	-0.080	0.072	-0.210	-0.025	0.076	0.033	-0.057	0.084	-0.158	1.214

Table 3 Transformations found for the registration of each couple of images. The value of the objective function of the best solution found, denoted by $C^*(\Phi(t))$, is also given.

As these algorithms are static, we have to consider the registration of each couple of successive images as a new problem to optimize. Thus, these algorithms are restarted after the registration of each couple of images, using the stagnation criterion defined in section 3.2. The results obtained using MLSDO, as a static optimization algorithm, are also given.

The parameters found for the elastic transformation model are given in Table 3. In Table 4, the average number of evaluations among 20 runs of the algorithms are given. The average of the best objective function values (see equation (15)) of each registration of the sequence is also given, averaged on 20 runs of the algorithms. The computational complexity of the registration method, using each algorithm, is also given in this table. The convergence of MLSDO, and that of the best performing static optimization algorithm on the problem at hand, *i.e.* CMA-ES, are illustrated by the curves in Figure 11. It shows the evolution of the relative error $\left(\frac{C^*(\Phi(t))-C(\Phi(t))}{C^*(\Phi(t))}\right)$ between the value of the objective function of the best solution found ($C^*(\Phi(t))$) and that of the current solution ($C(\Phi(t))$) for each couple of images (t). The presented curves give an idea about the convergence of the algorithms to an optimal value. It can also be seen as a stagnation metric of the algorithms. In this figure, the number of evaluations per registration of a couple of images is fixed to 5000, in order to enable the comparison of the convergence of the algorithms. For readability, a logarithmic scale is used on the ordinates.

As we can see, the average objective function value given in Table 4 shows that the algorithms have a similar average precision. However, we can see in Table 4 that the number of evaluations of the objective function performed by MLSDO, used as a dynamic optimization algorithm, is significantly lower than the ones of the static optimization algorithms. A Jarque-Bera statistical test has been applied on the num-

	Algorithm	Evaluations	$\sum_{t=1}^{19} \frac{C^*(\Phi(t))}{19}$	Complexity
Dynamic optimization	MLSDO	6880.68 ± 585.92	1.21 ± 7.0E-4	$O(n d^3)$
Static optimization	CMA-ES	7709.14 ± 467.75	1.21 ± 9.1E-4	$O(n d^2)$
	SPSO-07	8007.21 ± 364.24	1.21 ± 8.8E-4	$O(n d)$
	DE	9131.25 ± 279.20	1.21 ± 9.3E-4	$O(n d)$
	MLSDO	9522.76 ± 648.87	1.21 ± 1.7E-3	$O(n d^3)$

Table 4 Average number of evaluations to register a couple of images, and average value of $C^*(\Phi(t))$, obtained by each algorithm. The computational complexity of the registration method, using each algorithm, is also given, where n is the number of images in the sequence and d is the dimension of the search space.

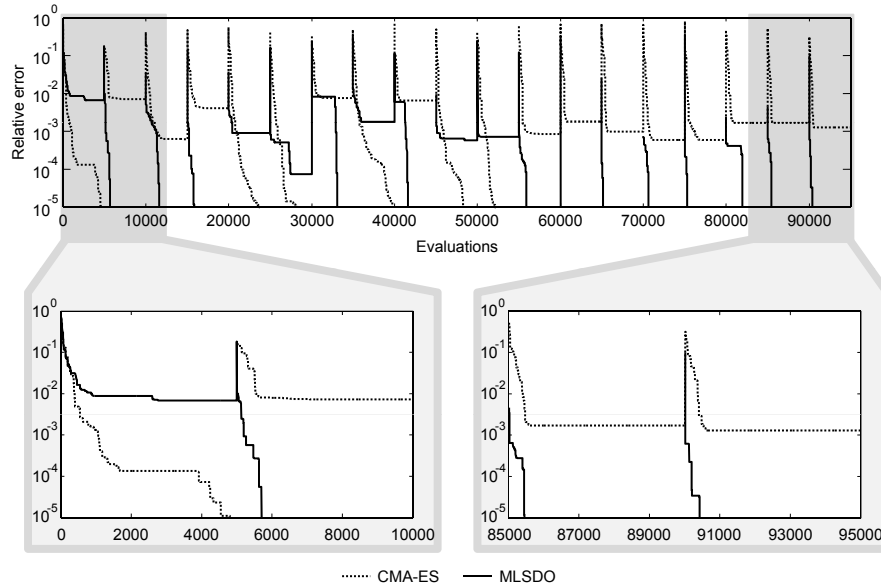


Fig. 11 Convergence graph of MLSDO and CMA-ES on the problem at hand.

bers of evaluations performed by the compared algorithms. This test indicates at a 95% confidence level that the numbers of evaluations follow a normal distribution. Then, we can perform a one-way ANOVA on these numbers of evaluations. This test confirms at a 95% confidence level that there is a significant difference between the performances of at least two of the compared algorithms. Then, the Tukey-Kramer multiple comparisons procedure has been used to determine which algorithms differ in terms of number of evaluations. It appears that MLSDO performs significantly differently from all the other tested algorithms. It can also be seen in Figure 11 that the convergence of MLSDO to an acceptable solution is faster than CMA-ES (the best performing static optimization algorithm on the problem at hand) for the registration of most of the couples of contours, especially for the last ones. MLSDO needs indeed to learn from the first registrations in order to accelerate its conver-

gence on the next ones. Thus, this comparison shows the efficiency of MLSDO and the significance of using a dynamic optimization algorithm on the problem at hand.

5 Conclusion

In this chapter, a registration process based on a dynamic optimization algorithm is proposed to register quickly all the images of a cine-MRI sequence. It takes profit from the effectiveness of the dynamic optimization paradigm. The process is sequentially applied on all the 2D images. The entire procedure is fully automated and provides an accurate assessment of the ROI deformation throughout the entire cardiac cycle. Our work under progress consists of the parallelization of the MLSDO algorithm using Graphics Processing Units.

References

- [1] S. Bird and X. Li. Using regression to improve local convergence. In *Proceedings of the IEEE Congress on Evolutionary Computation*, pages 592–599, Singapore, 2007. IEEE.
- [2] T. Blackwell and J. Branke. Multi-swarm optimization in dynamic environments. *Lecture Notes in Computer Science*, 3005:489–500, 2004.
- [3] T. Blackwell and J. Branke. Multi-swarms, exclusion and anti-convergence in dynamic environments. *IEEE Transactions on Evolutionary Computation*, 10(4):459–472, 2006.
- [4] J. Branke. The Moving Peaks Benchmark website. <http://www.aifb.uni-karlsruhe.de/~jbr/MovPeaks>, 1999.
- [5] J. Brest, A. Zamuda, B. Boskovic, M. S. Maucec, and V. Zumer. Dynamic optimization using self-adaptive differential evolution. In *Proceedings of the IEEE Congress on Evolutionary Computation*, pages 415–422, Trondheim, Norway, 2009. IEEE.
- [6] M. J. Budoff, N. Ahmadi, G. Sarraf, Y. Gao, D. Chow, F. Flores, and S. S. Mao. Determination of left ventricular mass on cardiac computed tomographic angiography. *Academic Radiology*, 16(6):726–732, 2009.
- [7] Y. Chenoune, E. Deléchelle, E. Petit, T. Goissen, J. Garot, and A. Rahmouni. Segmentation of cardiac cine-MR images and myocardial deformation assessment using level set methods. *Computerized Medical Imaging and Graphics*, 29(8):607–616, 2005.
- [8] S. Damas, O. Cerdón, and J. Santamaría. Medical image registration using evolutionary computation: A survey. *IEEE Computational Intelligence Magazine*, in press, 2011.
- [9] F. O. de França and F. J. Von Zuben. A dynamic artificial immune algorithm applied to challenging benchmarking problems. In *Proceedings of the IEEE*

- Congress on Evolutionary Computation*, pages 423–430, Trondheim, Norway, 2009. IEEE.
- [10] W. Du and B. Li. Multi-strategy ensemble particle swarm optimization for dynamic optimization. *Information Sciences*, 178(15):3096–3109, 2008.
 - [11] M. Clerc *et al.* The *Particle Swarm Central* website. <http://www.particleswarm.info>.
 - [12] N. Hansen and A. Ostermeier. Completely derandomized self-adaptation in evolution strategies. *Evolutionary Computation*, 9(2):159–195, 2001.
 - [13] P. Korosec and J. Silc. The differential ant-stigmergy algorithm applied to dynamic optimization problems. In *Proceedings of the IEEE Congress on Evolutionary Computation*, pages 407–414, Trondheim, Norway, 2009. IEEE.
 - [14] J. Lepagnot, A. Nakib, H. Oulhadj, and P. Siarry. A multiple local search algorithm for continuous dynamic optimization. Under submission.
 - [15] J. Lepagnot, A. Nakib, H. Oulhadj, and P. Siarry. Performance analysis of MADO dynamic optimization algorithm. In *Proceedings of the IEEE International Conference on Intelligent Systems Design and Applications*, pages 37–42, Pisa, Italy, 2009. IEEE.
 - [16] J. Lepagnot, A. Nakib, H. Oulhadj, and P. Siarry. A new multiagent algorithm for dynamic continuous optimization. *International Journal of Applied Metaheuristic Computing*, 1(1):16–38, 2010.
 - [17] C. Li and S. Yang. A generalized approach to construct benchmark problems for dynamic optimization. In *Proceedings of the 7th International Conference on Simulated Evolution and Learning*, pages 391–400, Melbourne, Australia, 2008. Springer.
 - [18] C. Li and S. Yang. A clustering particle swarm optimizer for dynamic optimization. In *Proceedings of the IEEE Congress on Evolutionary Computation*, pages 439–446, Trondheim, Norway, 2009. IEEE.
 - [19] C. Li, S. Yang, T. T. Nguyen, E. L. Yu, X. Yao, Y. Jin, H.-G. Beyer, and P. N. Suganthan. Benchmark generator for CEC 2009 competition on dynamic optimization. Technical report, University of Leicester, University of Birmingham, Nanyang Technological University, 2008.
 - [20] X. Li, J. Branke, and T. Blackwell. Particle swarm with speciation and adaptation in a dynamic environment. In *Proceedings of the Genetic and Evolutionary Computation Conference*, pages 51–58, Seattle, Washington, USA, 2006. ACM.
 - [21] L. Liu, S. Yang, and D. Wang. Particle swarm optimization with composite particles in dynamic environments. *IEEE Transactions on Systems, Man, and Cybernetics, Part B: Cybernetics*, 40(6):1634–1648, 2010.
 - [22] R. I. Lung and D. Dumitrescu. Collaborative evolutionary swarm optimization with a Gauss chaotic sequence generator. *Innovations in Hybrid Intelligent Systems*, 44:207–214, 2007.
 - [23] R. I. Lung and D. Dumitrescu. ESCA: A new evolutionary-swarm cooperative algorithm. *Studies in Computational Intelligence*, 129:105–114, 2008.
 - [24] J. B. A. Maintz and M. A. Viergever. A survey of medical image registration. *Medical Image Analysis*, 2(1):1–36, 1998.

- [25] R. Mendes and A. Mohais. DynDE: A differential evolution for dynamic optimization problems. In *Proceedings of the IEEE Congress on Evolutionary Computation*, pages 2808–2815, Edinburgh, Scotland, 2005. IEEE.
- [26] I. Moser and R. Chiong. Dynamic function optimisation with hybridised extremal dynamics. *Memetic Computing*, 2(2):137–148, 2010.
- [27] I. Moser and T. Hendtlass. A simple and efficient multi-component algorithm for solving dynamic function optimisation problems. In *Proceedings of the IEEE Congress on Evolutionary Computation*, pages 252–259, Singapore, 2007. IEEE.
- [28] A. Nakib, F. Aiboud, J. Hodel, P. Siarry, and P. Decq. Third brain ventricle deformation analysis using fractional differentiation and evolution strategy in brain cine-MRI. In *Medical Imaging 2010: Image Processing*, volume 7623, pages 762321–762321–10, San Diego, California, USA, 2010. SPIE.
- [29] P. Novoa, D. A. Pelta, C. Cruz, and I. G. del Amo. Controlling particle trajectories in a multi-swarm approach for dynamic optimization problems. In *Proceedings of the International Work-conference on the Interplay between Natural and Artificial Computation*, pages 285–294, Santiago de Compostela, Spain, 2009. Springer.
- [30] D. Parrott and X. Li. Locating and tracking multiple dynamic optima by a particle swarm model using speciation. *IEEE Transactions on Evolutionary Computation*, 10(4):440–458, 2006.
- [31] K. Price, R. Storn, and J. Lampinen. *Differential Evolution - A Practical Approach to Global Optimization*. Springer, 2005.
- [32] C. Studholme, D.L.G. Hill, and D.J. Hawkes. An overlap invariant entropy measure of 3D medical image alignment. *Pattern Recognition*, 32(1):71–86, 1999.
- [33] H. Sundar, H. Litt, and D. Shen. Estimating myocardial motion by 4D image warping. *Pattern Recognition*, 42(11):2514–2526, 2009.
- [34] S. Yang and C. Li. A clustering particle swarm optimizer for locating and tracking multiple optima in dynamic environments. *IEEE Transactions on Evolutionary Computation*, 14(6):959–974, 2010.
- [35] E. L. Yu and P. Suganthan. Evolutionary programming with ensemble of external memories for dynamic optimization. In *Proceedings of the IEEE Congress on Evolutionary Computation*, pages 431–438, Trondheim, Norway, 2009. IEEE.
- [36] B. Zitová and J. Flusser. Image registration methods: a survey. *Image and Vision Computing*, 21(11):977–1000, 2003.